SEAFORMER: A SPATIAL PROXIMITY AND EDGE-AWARE TRANSFORMER FOR REAL-WORLD VEHICLE ROUTING PROBLEMS

Anonymous authors
Paper under double-blind review

ABSTRACT

Real-world Vehicle Routing Problems (RWVRPs) require solving complex, sequence-dependent challenges at scale with constraints such as delivery time window, replenishment or recharging stops, asymmetric travel cost, etc. While recent neural methods achieve strong results on large-scale classical VRP benchmarks, they struggle to address RWVRPs because their strategies overlook sequence dependencies and underutilize edge-level information, which are precisely the characteristics that define the complexity of RWVRPs. We present SEAFormer, a novel transformer that incorporates both node-level and edge-level information in decision-making through two key innovations. First, our Clustered Proximity Attention (CPA) exploits locality-aware clustering to reduce the complexity of attention from $O(n^2)$ to $O(n)$ while preserving global perspective, allowing SEAFormer to efficiently train on large instances. Second, our lightweight edge-aware module captures pairwise features through residual fusion, enabling effective incorporation of edge-based information and faster convergence. Extensive experiments across four RWVRP variants with various scales demonstrate that SEAFormer achieves superior results over state-of-the-art methods. Notably, SEAFormer is the first neural method to solve 1,000+ node RWVRPs effectively, while also achieving superior performance on classic VRPs, making it a versatile solution for both research benchmarks and real-world applications.

1 INTRODUCTION

The Vehicle Routing Problem (VRP) is a fundamental challenge in logistics, where the goal is to deliver goods to many customers from a depot while minimizing cost and respecting constraints such as vehicle capacity. In practice, VRPs appear most prominently in last-mile deliveries, which have surged dramatically in recent years. For example, in 2022, Manhattan saw over 2.4 million delivery requests per day (Blueprint, 2022), averaging over 3,000 deliveries per minute during a 12-hour workday. Although existing solutions perform well on simplified benchmarks, they rarely account for the operational real-world problems, scales, and constraints encountered in practice.

Real-world Vehicle Routing Problems (RWVRPs) extend the VRP by incorporating sequence-dependent constraints. This class includes variants such as VRPTW (time window (Kallehauge et al., 2005)), EVRPCS (electric vehicles with recharging - which is important as carrying large weight significantly reduces their driving range (Szumska et al., 2021)), VRPRS (replenishment stops where vehicles can restock to continue service (Schneider et al., 2015)) and AVRP (asymmetric travel costs (Vigo, 1996)). Unlike the VRP, RWVRPs feature multi-dimensional constraints where routing decisions propagate through the entire system. For example, customer time windows impose strict temporal dependencies between stops, choosing a charging station affects subsequent sequences, asymmetric networks create cost imbalances between outbound and return legs, and replenishment stops extend vehicle capacity dynamically. These interdependencies transform the capacity-constrained spatial optimization problem of simple VRPs into a sequence-dependent one and form a tightly coupled setup that can only be validated by considering the entire route sequence.

Recent progress in deep learning has delivered impressive results for combinatorial optimization, reaching near-optimal solutions on classical VRP benchmarks. Existing approaches can be grouped

into two main paradigms: autoregressive and non-autoregressive models, each offering unique benefits and facing specific challenges when extended to RWVRPs.

Autoregressive methods (Kool et al., 2018; Kwon et al., 2020; Berto et al., 2025; Li et al., 2024; Lin et al., 2021; Chen et al., 2022; Wang et al., 2024) designed for VRP or RWVRPs, construct solutions sequentially using transformers and perform well on small-scale benchmarks. However, their performance deteriorates as problem size increases. They lack spatial inductive bias, treating all node pairs uniformly, disregarding the inherent geometric structure of routing problems. In addition, their full attention incurs an $O(n^2d)$ memory cost, where d is the embedding dimension, limiting training to hundreds rather than thousands of nodes. Moreover, they cannot represent edge-specific attributes (e.g., asymmetric costs, energy use, or traffic), limiting applicability to real-world routing where pairwise relationships drive feasibility and optimality. These architectural limitations make current autoregressive methods unsuitable for deployment on industrial-scale real-world routing problems.

Recent efforts to address the scalability limits of autoregressive models introduce new challenges when applied to RWVRPs. Divide-and-conquer methods (Hou et al., 2022; Nasehi et al., 2025; Zheng et al., 2024) can handle larger instances by decomposing the problem, yet they often overlook the sequential dependencies critical to RWVRPs, leading to infeasible or low-quality routes. Other scalable architectures (Gao et al., 2024; Luo et al., 2023; 2025a) face their own limitations, including substantial computational overhead or reliance on supervised learning which requires a set of precomputed optimal solutions that are themselves computationally expensive to obtain.

In contrast, non-autoregressive methods (Kool et al., 2022; Qiu et al., 2022) improve scalability by predicting all routing decisions simultaneously through learned heatmaps, thereby avoiding the sequential bottleneck of autoregressive decoding. While computationally efficient, these methods face a fundamental challenge similar to divide-and-conquer approaches: they cannot assess constraint satisfaction without the knowledge of the traversal sequence. Critical constraints, such as battery levels, are inherently path-dependent and require sequential state accumulation to ensure feasibility. As a result, non-autoregressive models are inherently hard to adapt to RWVRPs.

In this paper, we introduce **SEAFormer** (Spatial proximity and Edge-Aware transFormer), a novel architecture that combines the representational power required for RWVRPs with the computational efficiency necessary for real-world use. Unlike existing methods that treat routing as purely node selection, our model explicitly reasons about both *where to go* (nodes) and *how feasible/costly that transition is* (edges), a distinction critical for handling edge-level information and improving generalization. SEAFormer introduces two complementary innovations that together enable scalable, high-quality solutions across diverse RWVRP and VRP variants.

First, we propose **Clustered Proximity Attention (CPA)**, a spatially aware attention mechanism that improves generalization while reducing the complexity of full attention from $O(n^2)$ to $O(n)$. Unlike generic sparse attention methods (e.g., Longformer (Beltagy et al., 2020)), CPA leverages problem-specific spatial patterns to cluster nodes into meaningful partitions and applies attention within each partition. Our deterministic-yet-diverse clustering strategy offers multiple spatial perspectives, to avoid the local optima issues often encountered in sparse attention mechanisms.

Second, we introduce a **lightweight edge-aware module** that explicitly models pairwise relationships between nodes, capabilities largely absent from existing approaches. While node embeddings capture individual locations and demands, they cannot represent edge-specific attributes. Incorporating edge-level information not only enables solutions to problems where such details are essential but also enhances accuracy, generalization, and convergence across models. Our module learns these relational patterns through a parameter-efficient architecture (increasing number of parameters by only 7.5%), which is additively combined with the attention decoder to jointly optimize the problem. To the best of our knowledge, SEAFormer is the first unified approach to address this comprehensive range of real-world routing constraints at scales within a single architecture.

We evaluate SEAFormer on four RWVRP variants across a wide range of problem sizes and compare it with state-of-the-art neural and classical methods. For complex variants such as VRPTW, EVRPCS, VRPRS, and AVRP, it delivers at least 15% reduction in the objective value over the large-scale instances while fully respecting operational constraints. On standard VRP benchmarks, SEAFormer consistently surpasses the state-of-the-art approaches. Even on large-scale instances, SEAFormer preserves solution quality, whereas existing neural solvers often run out of memory or suffer substantial performance degradation.

The contributions of this paper are threefold. (i) We introduce SEAFormer, the first transformer to jointly optimize spatial proximity and edge-level constraints for real-world VRP variants, achieving state-of-the-art performance across different benchmarks. (ii) We propose Clustered Proximity Attention (CPA), a problem-specific sparse attention mechanism that leverages spatial locality in routing tasks, enhancing generalization and reducing memory complexity through deterministic-yet-diverse clustering. (iii) We propose a parameter-efficient edge-aware module that integrates pairwise relational information into routing decisions, enabling seamless handling of edge-specific constraints that are essential for real-world deployment yet missing from existing neural solvers.

2 Related work

We review existing learning-based approaches to RWVRPs and VRP, focusing on why they struggle to simultaneously achieve solution quality, computational efficiency, and constraint satisfaction at real-world scales. A more comprehensive discussion is provided in Appendix I.

2.1 Neural solvers with limited scalability

Autoregressive neural methods construct solutions sequentially using learned policies, with several notable approaches in the literature (Kool et al., 2018; Kwon et al., 2020; Berto et al., 2025; Luo et al., 2023). These models capture sequence dependencies during solution generation. While effective on small-scale problem instances, their performance deteriorates on large-scale problems. Moreover, reliance on the full-attention mechanism limits scalability and prevents efficient iterative refinement on standard hardware.

2.2 Scalable neural approaches

Recent approaches for scalable VRP solutions (Hou et al., 2022; Zheng et al., 2024; Nasehi et al., 2025; Ye et al., 2024) are based on divide-and-conquer method. Such techniques, however, cannot solve RWVRPs effectively as they cluster nodes before determining visit sequences, yet feasibility of a solution for RWVRPs depends on those sequences. Whether a vehicle can serve a cluster requires knowing its state upon arrival, such as battery level in EVRPCS or elapsed time in VRPTW, which is unavailable during clustering. This circular dependency causes clusters to violate constraints once sequenced, requiring expensive repairs or prevents finding high-quality solutions.

Scalable VRP solutions that do not rely on divide-and-conquer strategy face challenges when applied to RWVRPs. ELG (Gao et al., 2024) restricts attention to nearby nodes using distance-based penalties, which can limit performance in RWVRPs where vehicles need to reach distant nodes. Furthermore, the local attention approach does not explicitly account for RWVRP-specific constraints, which may lead to infeasible or suboptimal solutions. Heavy decoder architectures (Luo et al., 2023; 2025a) rely on supervised learning from near-optimal solutions. For RWVRPs, generating such training data is computationally expensive. For example, solving 100-node EVRPCS instances to optimality can be prohibitively time-consuming, and in some cases computationally infeasible, making these approaches impractical for RWVRPs.

Non-autoregressive models Ye et al. (2024); Qiu et al. (2022); Kool et al. (2022) generate high-quality solutions for large-scale VRPs by predicting edge inclusion probabilities via a heatmap. However, they face specific challenges with sequential constraints in RWVRPs. For instance, in EVRPCS, edge feasibility depends on the vehicle's battery state upon arrival, information that is unavailable during parallel prediction. Applying non-autoregressive methods to sequence-dependent problems requires costly repair procedures too, which often leads to a drop in solution quality.

2.2.1 RWVRP-specific methods

A few recent works directly address variations of RWVRPs. Lin et al. (2021) used Transformer-LSTM to track electric vehicle travel history, while Chen et al. (2022) employed GRUs with two-stage training to improve charging station routing. Wang et al. (2024) introduced a GAT-based encoder with penalty functions to enforce constraints for EVRPCS. Liu et al. (2024) and Berto et al. (2025) proposed multi-task learning for VRP variants such as VRPTW. Despite these advances, existing methods face at least one of the following limitations: (i) limited scalability, resulting in low-

quality solutions for instances larger than 100 nodes; (ii) reliance on manually tuned penalty terms, which slows training and may still produce infeasible solutions requiring costly post-processing; and (iii) sub-optimal strategies for visiting infrastructure nodes, limiting the model's ability to determine when and where to charge or restock efficiently, leading to lower quality solutions.

2.3 Sparse attention mechanisms

Recent advances in efficient attention offer potential solutions to scalability challenges. Reformer (Kitaev et al., 2020) leverages locality-sensitive hashing, Longformer (Beltagy et al., 2020) employs sliding windows, and BigBird (Zaheer et al., 2020) combines random, window, and global attention. These mechanisms are designed for text processing and do not naturally align with the geometric structure of routing problems and thus cannot be easily extended to spatial problems. While language tasks mainly involve local sequential dependencies, routing requires radial connectivity between depots and customers. Sparsity patterns based on these methods will disrupt the spatial relationships, limiting performance on routing tasks.

3 Clustered Proximity Attention

Figure 1 shows a VRP solution captured from Hou et al. (2022), highlighting an important structural pattern: nodes within the same route tend to cluster based on their polar coordinates relative to the depot. In particular, they typically follow one of three patterns: (1) similar angles but varying distances from the depot, (2) similar distances but different angles, or (3) close proximity in both angle and distance. This insight motivates our polar clustering approach, as optimal routes naturally reflect these geometric relationships.

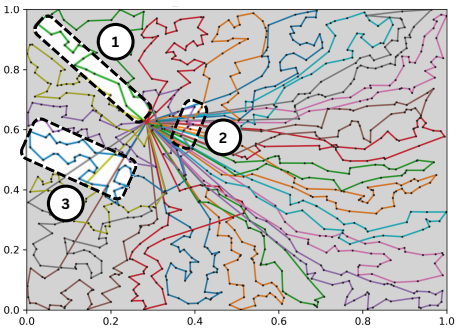

Figure 1: A VRP solution. Nodes within the same route can exhibit: (1) similar angles but different distances, (2) similar distances but different angles, or (3) a close proximity in both.

We propose **Clustered Proximity Attention (CPA)**, a problem-specific sparse attention mechanism that maintains spatial routing structure while substantially reducing computational complexity. The procedure is detailed below.

Polar-based Spatial Transformation. Given node coordinates $\{x_i \in \mathbb{R}^2\}_{i=0}^{n}$ with depot n_0, first we transform each customer location to polar coordinates:

$$r_i = \|x_i - x_0\|_2, \quad \theta_i = \arctan 2(y_i - y_0, x_i - x_0) \in [0, 2\pi), \tag{1}$$

where r_i represents radial distance and θ_i represents angular position relative to the depot.

Partitioning Score. To form clusters capturing the diverse spatial patterns illustrated in Figure 1 and necessary for optimal routing, we introduce a partitioning score that balances radial and angular proximity. After normalizing polar coordinates to $[0, 1]$, we compute a clustering metric as:

$$s_i^{(\alpha)} = \alpha \cdot \bar{\theta}_i + (1 - \alpha) \cdot \bar{r}_i, \tag{2}$$

where $\bar{r}_i = (r_i - r_{\min})/(r_{\max} - r_{\min})$ and $\bar{\theta}_i = \theta_i/2\pi$ represent the normalized radial and angular coordinates, respectively, and α is the mixing coefficient that controls the relative importance of distance versus angle in cluster formation.

Deterministic-yet-Diverse Partitioning. To prevent overfitting to specific cluster configurations, preserve global context, and capture diverse spatial patterns while maintaining training efficiency, we use R partitioning rounds with varied mixing coefficients, defining α in Equation 2 as:

$$\alpha = t/(R - 1), \quad t \in \{0, 1, \ldots, R - 1\}. \tag{3}$$

This creates a spectrum from radial ($\alpha = 0$, grouping nodes at similar distances from depot) to angular clustering ($\alpha = 1$, grouping nodes sharing a similar angle from the depot). Each configuration captures different spatial patterns shown in Figure 1, entails to a proper global prospective.

Boundary Smoothing for Robust Clustering. Hard cluster boundaries can artificially separate nearby nodes, disrupting natural customer groups. We address this through a boundary smoothing technique. After sorting the calculated partitioning scores $S_\alpha = [s_\alpha^1, \ldots, s_n^\alpha]$, given M as the cluster size (a user-defined parameter analyzed in Appendix F), we apply a circular shift as:

$$S'_\alpha = [s_\alpha^{\lfloor M/2 \rfloor + 1}, \ldots, s_\alpha^n, s_\alpha^1, \ldots, s_\alpha^{\lfloor M/2 \rfloor}] \tag{4}$$

This rotation softens the deterministic cluster boundaries that would otherwise push nearby nodes apart, keeping close nodes together and improving transitions between clusters. After computing the partitioning scores $S = \{S_{\alpha_1}, S'_{\alpha_1}, S_{\alpha_2}, ...\}$ across different proximity weights and rotations, we partition nodes into clusters of size M based on each score. A comprehensive description with visual examples of CPA is provided in Appendix H.

Localized Attention Computation. Given partition $\mathcal{P} = \{C_{\alpha_1}^1, C_{\alpha_1}^2, \ldots, C_{\alpha_1}^k, \ldots\}$ where each C_α^j contains M proximate nodes, we compute attention independently within each cluster as:

$$\text{Attention}(Q_j, K_j, V_j) = \text{softmax}\left(\frac{Q_j K_j^\top}{\sqrt{d}}\right) V_j, \quad \text{where } Q_j, K_j, V_j \in \mathbb{R}^{|C_\alpha^j| \times d}. \tag{5}$$

Complexity analysis: CPA reduces complexity of attention from $O(n^2)$ to $O(n)$ while preserving the spatial relationships critical for routing decisions. It partitions nodes into clusters of size M. Each cluster requires $O(M^2)$ operations for attention computation. With $\lceil n/M \rceil$ clusters total:

$$\text{CPA complexity} = O\Big(\underbrace{R}_{\text{No. rounds}} \times \underbrace{\lceil n/M \rceil}_{\text{clusters}} \times \underbrace{(M^2)}_{\text{per cluster}} \Big) = O(nRM) = O(n) \tag{6}$$

4 SEAFORMER ARCHITECTURE

Figure 2 shows the SEAFormer architecture, a dual-stream design that jointly models node-level spatial structure and edge-level information for RWVRPs. The node stream encodes location features using our Clustered Proximity Attention (presented in Section 3), while the edge-aware stream maintains explicit embeddings for pairwise attributes such as costs and distances. These two streams converge in the decoder: node embeddings drive the sequential step-by-step node selection, and edge embedding is used to rank candidate transitions from the current position through a learned heatmap generation. This separation of roles allows SEAFormer to scale to thousands of nodes, converge faster, and remain expressive enough to handle complex real-world constraints. The encoder of SEAFormer comprises two complementary modules.

Node embedding through CPA. This module adopts the encoder architecture from Kwon et al. (2020), encoding node features through L layers. Unlike prior works that employ full attention mechanisms, SEAFormer utilizes CPA to produce spatially-aware node embeddings $H_n \in \mathbb{R}^{n \times d}$, while achieving significant memory savings in training and inference.

For problem variants with optional service nodes such as EVRPCS (charging stations) and VRPRS (replenishment stops), we augment the spatial encoder with a specialized optional node processing pathway. This parallel encoding layer generates embeddings for optional nodes $H_o \in \mathbb{R}^{f \times d}$, where f represents the number of service facilities. These embeddings are then fused with customer embeddings through a learnable mechanism, and the combined representations pass through the same batch normalization and feed-forward layers. This allows each customer embedding to account for nearby optional facilities and their influence on route feasibility, which is crucial in problems where strategic service stops can substantially enhance or even enable high-quality solutions. A comprehensive description of the optional node embedding and integration mechanism is provided in Appendix G.

Edge-Aware Embedding Module. We design our edge embedding to preserve the properties that exist for edges while maintaining computational efficiency. The edge-aware embedding module only operates on edges between depots and customers, while optional nodes in EVRPCS and VRPRS do not participate in this process. Given edge features (distance, energy consumption rate, historical

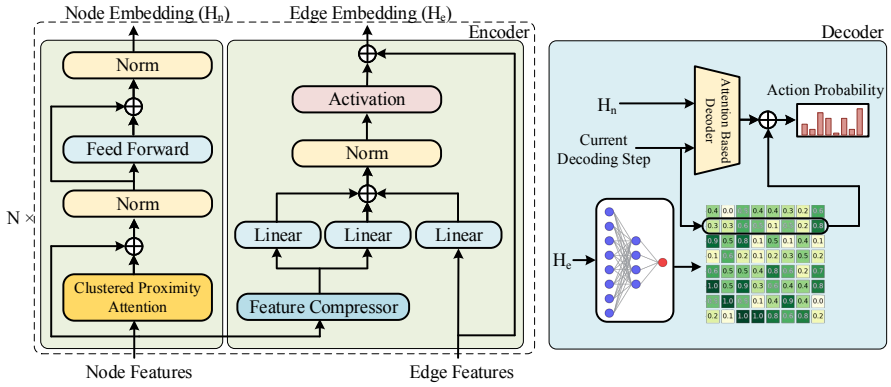

Figure 2: SEAFormer Architecture. The dual-module encoder embeds nodes through CPA and edges through a lightweight residual module. The dual-path decoder combines edge-aware guidance (heatmap) with sequential node selection (attention), unified through logit fusion. This design enables scalable training on large number of nodes while handling diverse RWVRP constraints.

traffic) embedding $X_e^{(i,j)} \in \mathbb{R}^{d_e}$, and node embeddings $H_n^{(i)}, H_n^{(j)} \in \mathbb{R}^d$, we compute edge-aware embeddings through residual fusion (Szegedy et al., 2017):

$$H_e^{(i,j)} = X_e^{(i,j)} + \sigma\left(\text{BN}\left(W_1 H_n^{(i)} + W_2 H_n^{(j)} + W_3 X_e^{(i,j)}\right)\right) \tag{7}$$

Where W is a trainable parameter, $W_1 H_n^{(i)}$ captures origin-specific factors, $W_2 H_n^{(j)}$ captures destination-specific factors, $W_3 X_e^{(i,j)}$ captures edge features. Prior to this, we apply a linear transformation to reduce node features to match edge embedding dimensions, enabling the model to extract only relative information from node embeddings. Batch normalization ensures stable training across diverse edge scales and SILU activation (σ) enables modeling of complex non-linear relationships. This architecture anchors edge representations in spatial context while increasing the model's total parameters by only 7.5%. Lastly, a residual connection maintains original edge information while selectively integrating node-level context.

Once edge and node embeddings are generated, SEAFormer's decoder constructs the solution through dual complementary pathways that balance global optimization with sequential decoding.

Edge-Guided Global Heatmap. Before sequential decoding, we produce a static heatmap that encodes global edge preferences. This step occurs once at the onset of the decoding process:

$$\mathcal{H}_{ij} = tanh\big(\text{MLP}_\theta(H_e^{(i,j)})\big) \in \mathbb{R}, \quad \forall i, j \in \{1, \ldots, n\}, \tag{8}$$

where MLP_θ is a multi-layer perceptron that maps each edge to a scalar score, followed by the $\tanh$ activation function. This module encodes edge features (e.g., travel times, distances) that are impossible to capture through node-level encoding.

Node-Guided Sequential Attention. The sequential decoder constructs solutions autoregressively, selecting one node at each step t based on the current state of the partially generated solution. To enable the model to differentiate between vehicle states across problem variants, we adapt the query vector to each RWVRP variant's state representation $\mathbf{q}_t = [\mathbf{h}_t; c_t; \xi_t]$, where $\mathbf{h}_t$ is the last visited node embedding and ξ_t represents variant-specific constraints: none for VRP, battery level b_t for EVRPCS, remaining travel length τ_t for VRPRS, and current time w_t for VRPTW. To ensure stable convergence and prevent bias from large values, we normalize ξ_t by its maximum value to maintain the range $[0, 1]$. Finally, the attention mechanism computes compatibility scores with all unvisited nodes through:

$$\alpha_{ti} = \begin{cases} \frac{\exp(\mathbf{q}_t^\top \mathbf{k}_i / \sqrt{d})}{\sum_{j \in \mathcal{U}_t} \exp(\mathbf{q}_t^\top \mathbf{k}_j / \sqrt{d})} & \text{if } i \in \mathcal{U}_t \\ 0 & \text{otherwise} \end{cases} \tag{9}$$

where $\mathcal{U}_t$ denotes the set of unvisited feasible nodes. We implement a proactive masking function that enhances solution quality, reduces search space, and prevents the model from generating infeasible solutions during inference (see Appendix B for detailed description). Finally, at each step t, we combine logits from both paths:

$$\ell_t = \ell_t^{\text{seq}} + \mathcal{H}_{i_t,:}, \tag{10}$$

where ℓ_t^{seq} is sequential attention logits, $\mathcal{H}_{i_t,:}$ is the heatmap row for current node i_t. For optional nodes not included in the heatmap, we define heatmap values as $\mathcal{H}_{i_t,j} = -2 \cdot \frac{r_t}{R_{\max}}, \quad j \in \mathcal{O}$ to encourage model to visit such nodes more frequently as resources deplete. Here, r_t denotes the remaining resource level (battery charge in EVRPCS or available driving range in VRPRS), $R_{\max}$ represents the maximum resource capacity (full battery capacity in EVRPCS or maximum driving range in VRPRS), and $\mathcal{O}$ denotes the set of optional nodes.

5 Experiments

To verify the applicability of SEAFormer on different variations of RWVRP and VRP, we evaluate SEAFormer on 5 combinatorial optimization problems, including VRPTW, EVRPCS, VRPRS, AVRP, and VRP. Detailed formulations of these problems are provided in Appendix A.

Benchmarks. We evaluate SEAFormer across four datasets: (i) Random RWVRP benchmarks, comprising 100 instances per problem size with up to 7K nodes (results up to 1k are shown in table 1, and larger values in appendix C) following Kwon et al. (2020); Zhou et al. (2023); (ii) Random VRP benchmarks with up to 7K nodes following Zhou et al. (2023); (iii) real-world VRP instances from CVRPLib; (iv) cross-distribution datasets generated by Zhou et al. (2023).

Implementation. For all problems, we train the model for 2000 epochs on 100-customer instances, then 200 epochs on 500-customer instances, and 100 epochs on 1000-customer instances. As in prior work, problem instances are uniformly sampled from the $[0, 1]^2$ space, and demands drawn from a discrete uniform distribution on $[1, 10]$. Asymmetric VRPs are created using our dataset generation procedure (refer to appendix A.4.1). The Adam optimizer (Kingma, 2014) is employed for training, with detailed hyperparameters for each problem provided in Appendix J.

Metrics. We report the mean objective (Obj.), gap (G), and inference time (T) for each approach. Objective represents solution length, where lower values signify superior performance. Gap quantifies the deviation from solutions generated by one of OR-tools, LKH, or HGS. Time denotes the total runtime across the entire dataset, measured in seconds (s), minutes (m), or hours (h). Runtimes, measured on identical hardware (NVIDIA A100 GPU for neural methods, 32-core CPU for classical solvers), exclude model loading and represent the total solution time over each dataset.

Inference. In the inference phase, we evaluate SEAFormer using two strategies. First, greedy decoding with 8-fold augmentation, and second, Simulation-Guided Beam Search (SGBS) (Choo et al., 2022), which requires additional computation time but yields superior results as it explores multiple solution trajectories simultaneously. The greedy variant of SEAFormer operates significantly faster than the SGBS version at the expense of marginally reduced solution quality.

Baselines. We compare SEAFormer with **1) Classical Solvers:** HGS (Vidal, 2022), LKH (Helsgaun, 2017), and OR-Tools; **2) Construction-based NCO Methods:** POMO (Kwon et al., 2020), MTPOMO (Liu et al., 2024), EVRPRL (Lin et al., 2021), EVGAT (Wang et al., 2024), LEHD (Luo et al., 2023), RELD (Huang et al., 2025), ELG (Gao et al., 2024) L2C-insert (Luo et al., 2025b), BLEHD (Luo et al., 2025a), and RouteFinder Berto et al. (2025); **3) Divide-and-conquer based methods:** GLOP (Ye et al., 2024), DeepMDV (Nasehi et al., 2025), UDC (Zheng et al., 2024). Not all existing methods apply to every RWVRP variant, so comparisons are limited to applicable approaches. For details on baselines and their integration, see Appendix K.

5.1 Evaluation on RWVRPs

Table 1 presents a comprehensive evaluation of SEAFormer against state-of-the-art methods across four challenging RWVRPs. SEAFormer consistently achieves superior or competitive performance across all problem variants and scales. Notably, using SGBS as a search method, SEAFormer establishes new state-of-the-art results in learning-based methods across all 12 test configurations between, at the cost of higher processing time, particularly with impressive gains on larger instances.

Table 1: Objective function (Obj.), Gap to the OR-tools (Gap), and solving time (Time) on 100, 500, and 1,000-node RWVRPs. All test sets contain 100 instances following settings in Zhou et al. (2023). The overall best performance is in bold and the best learning method is marked by shade. OR-Tools results are not optimal, as execution was stopped early due to time limits.

RWVRP	Methods	100 Customers			500 Customers			1K Customers		
		Obj.↓	G(%)	T	Obj.↓	G(%)	T	Obj.↓	G(%)	T
VRPTW	OR-Tools	**26.34**	**0.00**	1H	87.3	0.00	5H	151.4	0.00	10H
	POMO	26.81	1.78	5S	93.2	6.75	30S	193.2	27.6	1M
	MTPOMO	27.02	2.58	5S	96.8	10.8	30S	207.1	36.7	1M
	RouteFinder	26.8	1.74	5S	91.2	4.46	30S	171.4	11.3	1M
	SEAFormer	26.75	1.55	5S	87.4	0.11	30S	149.7	-1.1	1M
	SEAFormer-SGBS	26.5	0.6	10S	**85.0**	**-2.6**	13M	**145.2**	**-4.1**	1.6H
EVRPCS	OR-Tools	16.35	0.00	1H	31.1	0.00	5H	47.8	0.00	10H
	EVRPRL	16.54	1.16	10S	34.3	10.3	90S	62.1	29.9	3M
	EVGAT	16.9	3.36	30S	35.2	13.2	3M	56.3	17.8	6M
	SEAFormer	16.36	0.06	5S	30.8	-1.0	30S	45.8	-4.2	1M
	SEAFormer-SGBS	**16.14**	**-1.3**	15S	**30.2**	**-2.9**	13M	**44.9**	**-6.1**	1.7H
VRPRS	OR-Tools	11.2	0.00	1H	23.4	0.00	5H	36.11	0.00	10H
	EVRPRL	11.43	2.05	10S	25.16	7.52	90S	47.5	31.5	3M
	EVGAT	11.76	5.0	30S	25.65	9.6	3M	42.1	16.6	6M
	SEAFormer	11.24	0.35	5S	22.93	-2.0	30S	34.87	-3.4	1M
	SEAFormer-SGBS	**10.97**	**-2.0**	15S	**22.33**	**-4.6**	13M	**33.95**	**-6.0**	1.7H
AVRP	OR-Tools	19.37	0.00	1H	40.27	0.00	5H	47.6	0.00	10H
	POMO	19.5	0.7	10S	42.12	4.59	20S	53.44	12.3	1M
	MTPOMO	19.63	1.3	10S	44.4	10.2	3M	56.2	18.1	1M
	RouteFinder	19.6	1.2	5S	41.52	3.1	20S	48.3	1.47	1M
	LEHD	19.96	3.0	5S	40.71	1.1	20S	45.89	-3.6	1.2M
	BLEHD-PRC50	-	-	-	42.13	4.61	2.5M	45.23	-5.0	6M
	$UDC_{250}(\alpha = 50)$	-	-	-	40.06	-0.5	30M	45.17	-5.1	1.2H
	SEAFormer	19.48	0.6	5S	40.23	-0.1	30S	45.14	-5.2	1M
	SEAFormer-SGBS	**19.04**	**-1.7**	10S	**38.97**	**-3.2**	13M	**44.07**	**-7.4**	1.7H

While SEAFormer achieves superior performance on VRPTW, EVRPCS, and VRPRS across all settings where existing large-scale solutions fail, the AVRP results especially showcase SEAFormer's architectural strengths. Whereas learning-based approaches including POMO, LEHD, BLEHD, and UDC struggle with asymmetric distance matrices and show gaps up to 3% with OR-Tools on 100-customer instances, SEAFormer achieves the best performance with a 1.7% improvement over OR-Tools and increasingly larger gains on bigger instances. This highlights our model's superior capacity to capture complex spatial dependencies inherent in asymmetric routing problems.

The results highlight SEAFormer's exceptional scalability: while most baselines suffer severe degradation on 1,000-customer RWVRPs, SEAFormer preserves solution quality and remains the fastest method. The SGBS variant, though requiring additional computation (95-100 minutes for 1k customers), consistently produces the best solutions across all scales, suggesting an effective trade-off between solution quality and computational resources.

5.2 Evaluation on VRP

Table 2 reports SEAFormer's performance on standard VRP instances with 100–1000 customers, showing both strong scalability and high solution quality. On small instances, SEAFormer achieves 0.96% gap in 5 seconds, and with SGBS it matches POMO while retaining efficient inference. The advantage becomes clearer at larger scales: on 500-customer instances, our base model achieves a 4.64% gap in 15 seconds, which outperforms POMO and rivaling methods like DeepMDV-LKH3 that requires substantially more time. With SGBS, SEAFormer further improves to a 2.98% gap, surpassing all learning-based approaches. On the challenging 1,000-customer setting, where most neural methods degrade, SEAFormer proves robust, achieving a 0.62% gap in 30 seconds, surpassing LEHD (1.05% in 2 minutes) and very recent methods such as RELD (2.36%) and L2C-Insert (0.82%). With SGBS, SEAFormer outperforms HGS by a 0.9% gap and matches UDC and BLEHD.

Moreover, we evaluate SEAFormer on benchmarks across very large-scale (Appendix C), real-world (Appendix D), and cross-distribution (Appendix E) settings. In all cases, SEAFormer performs well, establishing itself as a robust solution for research benchmarks and real-world applications.

Table 2: Performance comparison of various methods on 100 VRP instances with 100, 500, and 1,000 customers. Best values are bolded while the best learning-based solutions are highlighted.

METHODS	100 CUSTOMERS			500 CUSTOMERS			1K CUSTOMERS		
	OBJ.↓	G(%)	T	OBJ.↓	G(%)	T	OBJ.↓	G(%)	T
HGS	**15.5**	**0.00**	40M	**36.84**	**0.00**	4H	43.5	0.00	8H
POMO	15.72	1.41	5S	44.8	21.6	20S	101	132	3M
GLOP-LKH3	21.3	36.5	30S	42.45	15.22	3M	45.9	5.51	2M
DEEPMDV-LKH3	16.2	4.51	90S	40.2	9.12	4M	45.0	3.44	8M
ELG	15.8	1.93	30S	38.34	4.07	2.6M	43.58	0.18	15M
LEHD	16.2	4.51	5S	38.41	4.26	20S	43.96	1.05	2M
BLEHD-PRC50	-	-	-	41.50	12.64	2.5M	43.13	-0.8	6M
RELD	15.75	1.61	5S	38.33	4.04	30S	44.53	2.36	50S
L2C-INSERT	15.72	1.41	2M	38.72	5.1	7M	43.86	0.82	13M
$UDC_{50}(\alpha = 50)$	-	-	-	38.34	4.07	7M	43.48	0.00	14M
$UDC_{250}(\alpha = 50)$	-	-	-	37.99	3.12	30M	**43.00**	**-1.1**	1.2H
SEAFORMER	15.82	2.06	5S	38.55	4.64	15S	43.77	0.62	30S
SEAFORMER-SGBS	15.72	1.41	30S	37.94	2.98	12M	43.10	-0.9	1.5H

5.3 ABLATION STUDY

Figure 3 shows that the edge module is crucial for SEAFormer's performance. With edge embeddings, SEAFormer converges faster than POMO; without them, convergence lags behind the baseline. This occurs because clustering modules like CPA inherently slow convergence by partitioning the attention space. The edge module compensates for this limitation, creating a complementary architecture where clustering handles scalability while edge embeddings accelerate learning.

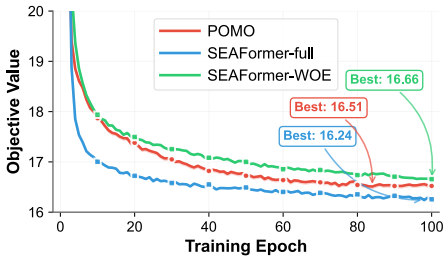

Figure 3: SEAFormer training with/without edge embeddings vs. POMO on VRP-100.

Table 3: Performance comparison of CPA versus alternative clustering approaches. Attention is applied within each cluster while keeping all other parameters in SEAFormer fixed. Gaps are w.r.t full SEAFormer with CPA clustering.

Method	VRP100	VRP500	VRP1000
Reformer-LSH4	0.3%	0.54%	1.27%
K-Means (one round)	7.8%	17.2%	28.7%
K-Means (four round)	2.6%	3.4%	3.9%
Grid-based clustering	8.14%	15.76%	24.05%

To validate CPA's effectiveness, we replace it with alternative clustering strategies in SEAFormer (Table 3). Reformer with LSH4 yields the smallest gap (0.3–1.27%), showing hash-based clustering can be competitive, though CPA remains superior. Multi-round K-Means improves over single-round, reducing the gap from 28.7% to 3.9% on VRP1000, underscoring the importance of iterative refinement. Grid-based clustering performs poorly, with up to 24.05% gap on VRP1000. These results confirm CPA's advantage for routing. For a more extensive ablation study, see Appendix F.

6 CONCLUSION

In this paper, we present SEAFormer, a scalable, edge-aware transformer for VRP and RWVRP variants that integrates Clustered Proximity Attention with a lightweight edge module. SEAFormer outperforms state-of-the-art RWVRP methods by at least 15% on large-scale instances, converges quickly, and performs well on standard VRPs. While current implementations primarily use greedy decoding, future work will explore high performance search in the heatmap and integrate learning-based partial solution construction to further improve solution quality and scalability.

REFERENCES

Irwan Bello, Hieu Pham, Quoc V Le, Mohammad Norouzi, and Samy Bengio. Neural combinatorial optimization with reinforcement learning. *arXiv preprint arXiv:1611.09940*, 2016.

Iz Beltagy, Matthew E Peters, and Arman Cohan. Longformer: The long-document transformer. *arXiv preprint arXiv:2004.05150*, 2020.

Federico Berto, Chuanbo Hua, Nayeli Gast Zepeda, André Hottung, Niels Wouda, Leon Lan, Junyoung Park, Kevin Tierney, and Jinkyoo Park. Routefinder: Towards foundation models for vehicle routing problems. *arXiv preprint arXiv:2406.15007*, 2025.

E-Commerce Blueprint. In NY daily news: Manhattan BP calls for delivery reforms as NYC residents, businesses receive more than 2.4 million packages per day. https://shorturl.at/1hX8B, 2022.

Jinbiao Chen, Huanhuan Huang, Zizhen Zhang, and Jiahai Wang. Deep reinforcement learning with two-stage training strategy for practical electric vehicle routing problem with time windows. In *International Conference on Parallel Problem Solving from Nature*, pp. 356–370. Springer, 2022.

Jinho Choo, Yeong-Dae Kwon, Jihoon Kim, Jeongwoo Jae, André Hottung, Kevin Tierney, and Youngjune Gwon. Simulation-guided beam search for neural combinatorial optimization. *Advances in Neural Information Processing Systems (NeurIPS)*, 35:8760–8772, 2022.

Tri Dao, Dan Fu, Stefano Ermon, Atri Rudra, and Christopher Ré. Flashattention: Fast and memory-efficient exact attention with io-awareness. *Advances in Neural Information Processing Systems (NeurIPS)*, 35:16344–16359, 2022.

Ángel Felipe, M Teresa Ortuño, Giovanni Righini, and Gregorio Tirado. A heuristic approach for the green vehicle routing problem with multiple technologies and partial recharges. *Transportation Research Part E: Logistics and Transportation Review*, 71:111–128, 2014.

Zhang-Hua Fu, Kai-Bin Qiu, and Hongyuan Zha. Generalize a small pre-trained model to arbitrarily large tsp instances. In *Proceedings of the AAAI Conference on Artificial Intelligence (AAAI)*, volume 35, pp. 7474–7482, 2021.

Chengrui Gao, Haopu Shang, Ke Xue, Dong Li, and Chao Qian. Towards generalizable neural solvers for vehicle routing problems via ensemble with transferrable local policy. In *Proceedings of the Thirty-Third International Joint Conference on Artificial Intelligence (IJCAI)*, 2024.

Keld Helsgaun. An extension of the lin-kernighan-helsgaun tsp solver for constrained traveling salesman and vehicle routing problems. *Roskilde: Roskilde University*, 12:966–980, 2017.

Qingchun Hou, Jingwei Yang, Yiqiang Su, Xiaoqing Wang, and Yuming Deng. Generalize learned heuristics to solve large-scale vehicle routing problems in real-time. In *The Eleventh International Conference on Learning Representations (ICLR)*, 2022.

Ziwei Huang, Jianan Zhou, Zhiguang Cao, and Yixin XU. Rethinking light decoder-based solvers for vehicle routing problems. In *The Thirteenth International Conference on Learning Representations (ICLR)*, 2025.

Eric Jang, Shixiang Gu, and Ben Poole. Categorical reparameterization with gumbel-softmax. *arXiv preprint arXiv:1611.01144*, 2016.

Chaitanya K Joshi, Thomas Laurent, and Xavier Bresson. On learning paradigms for the travelling salesman problem. *arXiv preprint arXiv:1910.07210*, 2019.

Brian Kallehauge, Jesper Larsen, Oli BG Madsen, and Marius M Solomon. Vehicle routing problem with time windows. In *Column Generation*, pp. 67–98. Springer, 2005.

Surendra Reddy Kancharla and Gitakrishnan Ramadurai. An adaptive large neighborhood search approach for electric vehicle routing with load-dependent energy consumption. *Transportation in Developing Economies*, 4:1–9, 2018.

Elias Khalil, Hanjun Dai, Yuyu Zhang, Bistra Dilkina, and Le Song. Learning combinatorial optimization algorithms over graphs. *Advances in Neural Information Processing Systems (NeurIPS)*, 30, 2017.

Diederik P Kingma. Adam: A method for stochastic optimization. *arXiv preprint arXiv:1412.6980*, 2014.

Nikita Kitaev, Lukasz Kaiser, and Anselm Levskaya. Reformer: The efficient transformer. In *International Conference on Learning Representations (ICLR)*, 2020.

Çağrı Koç, Ola Jabali, Jorge E Mendoza, and Gilbert Laporte. The electric vehicle routing problem with shared charging stations. *International Transactions in Operational Research*, 26(4):1211–1243, 2019.

Wouter Kool, Herke van Hoof, and Max Welling. Attention, learn to solve routing problems! In *International Conference on Learning Representations (ICLR)*, 2018.

Wouter Kool, Herke van Hoof, Joaquim Gromicho, and Max Welling. Deep policy dynamic programming for vehicle routing problems. In *International Conference on Integration of Constraint Programming, Artificial Intelligence, and Operations Research*, pp. 190–213, 2022.

Yeong-Dae Kwon, Jinho Choo, Byoungjip Kim, Iljoo Yoon, Youngjune Gwon, and Seungjai Min. POMO: Policy optimization with multiple optima for reinforcement learning. *Advances in Neural Information Processing Systems (NeurIPS)*, 33:21188–21198, 2020.

Jinqi Li, Bing Tian Dai, Yunyun Niu, Jianhua Xiao, and Yaoxin Wu. Multi-type attention for solving multi-depot vehicle routing problems. *IEEE Transactions on Intelligent Transportation Systems (TITS)*, 2024.

Sirui Li, Zhongxia Yan, and Cathy Wu. Learning to delegate for large-scale vehicle routing. *Advances in Neural Information Processing Systems (NeurIPS)*, 34:26198–26211, 2021.

Bo Lin, Bissan Ghaddar, and Jatin Nathwani. Deep reinforcement learning for the electric vehicle routing problem with time windows. *IEEE Transactions on Intelligent Transportation Systems (TITS)*, 23(8):11528–11538, 2021.

Fei Liu, Xi Lin, Zhenkun Wang, Qingfu Zhang, Tong Xialiang, and Mingxuan Yuan. Multi-task learning for routing problem with cross-problem zero-shot generalization. In *Proceedings of the 30th ACM Conference on Knowledge Discovery and Data Mining (SIGKDD)*, pp. 1898–1908, 2024.

Fu Luo, Xi Lin, Fei Liu, Qingfu Zhang, and Zhenkun Wang. Neural combinatorial optimization with heavy decoder: Toward large scale generalization. *Advances in Neural Information Processing Systems (NeurIPS)*, 36:8845–8864, 2023.

Fu Luo, Xi Lin, Yaoxin Wu, Zhenkun Wang, Tong Xialiang, Mingxuan Yuan, and Qingfu Zhang. Boosting neural combinatorial optimization for large-scale vehicle routing problems. In *The Thirteenth International Conference on Learning Representations (ICLR)*, 2025a.

Fu Luo, Xi Lin, Mengyuan Zhong, Fei Liu, Zhenkun Wang, Jianyong Sun, and Qingfu Zhang. Learning to insert for constructive neural vehicle routing solver. *Advances in Neural Information Processing Systems (NeurIPS)*, 2025b.

Michalis Mavrovouniotis, Georgios Ellinas, and Marios Polycarpou. Ant colony optimization for the electric vehicle routing problem. In *2018 IEEE Symposium series on computational intelligence (SSCI)*, pp. 1234–1241. IEEE, 2018.

Saeed Nasehi, Farhana Choudhury, Egemen Tanin, and Majid Sarvi. Deepmdv: Global spatial matching for multi-depot vehicle routing problems. *International Conference on Advances in Geographic Information Systems (SIGSPATIAL)*, 2025.

Mohammadreza Nazari, Afshin Oroojlooy, Lawrence Snyder, and Martin Takác. Reinforcement learning for solving the vehicle routing problem. *Advances in Neural Information Processing Systems (NeurIPS)*, 31, 2018.

Alex Nowak, David Folqué, and Joan Bruna. Divide and conquer networks. In *International Conference on Learning Representations (ICLR)*, 2018.

Ruizhong Qiu, Zhiqing Sun, and Yiming Yang. Dimes: A differentiable meta solver for combinatorial optimization problems. *Advances in Neural Information Processing Systems (NeurIPS)*, 35: 25531–25546, 2022.

Michael Schneider, Andreas Stenger, and Dominik Goeke. The electric vehicle-routing problem with time windows and recharging stations. *Transportation Science*, 48(4):500–520, 2014.

Michael Schneider, Andreas Stenger, and Julian Hof. An adaptive vns algorithm for vehicle routing problems with intermediate stops. *Or Spectrum*, 37:353–387, 2015.

Christian Szegedy, Sergey Ioffe, Vincent Vanhoucke, and Alexander Alemi. Inception-v4, inception-resnet and the impact of residual connections on learning. In *Proceedings of the AAAI Conference on Artificial Intelligence (AAAI)*, volume 31, 2017.

Emilia M Szumska, Rafał S Jurecki, and Rafał S Jurecki. Parameters influencing on electric vehicle range. *Energies*, 14(16):4821, 2021.

Paolo Toth and Daniele Vigo. A heuristic algorithm for the symmetric and asymmetric vehicle routing problems with backhauls. *European Journal of Operational Research*, 113(3):528–543, 1999.

Thibaut Vidal. Hybrid genetic search for the cvrp: Open-source implementation and swap* neighborhood. *Computers & Operations Research*, 140:105643, 2022.

Daniele Vigo. A heuristic algorithm for the asymmetric capacitated vehicle routing problem. *European Journal of Operational Research*, 89(1):108–126, 1996.

Mengqin Wang, Yanling Wei, Xueliang Huang, and Shan Gao. An end-to-end deep reinforcement learning framework for electric vehicle routing problem. *IEEE Internet of Things Journal*, 2024.

Niels A. Wouda, Leon Lan, and Wouter Kool. PyVRP: a high-performance VRP solver package. *INFORMS Journal on Computing*, 2024. URL https://doi.org/10.1287/ijoc.2023.0055

Yubin Xiao, Di Wang, Boyang Li, Mingzhao Wang, Xuan Wu, Changliang Zhou, and You Zhou. Distilling autoregressive models to obtain high-performance non-autoregressive solvers for vehicle routing problems with faster inference speed. In *Proceedings of the AAAI Conference on Artificial Intelligence (AAAI)*, volume 38, pp. 20274–20283, 2024.

Liang Xin, Wen Song, Zhiguang Cao, and Jie Zhang. Multi-decoder attention model with embedding glimpse for solving vehicle routing problems. In *Proceedings of the AAAI Conference on Artificial Intelligence (AAAI)*, volume 35, pp. 12042–12049, 2021.

Haoran Ye, Jiarui Wang, Helan Liang, Zhiguang Cao, Yong Li, and Fanzhang Li. GLOP: Learning global partition and local construction for solving large-scale routing problems in real-time. In *Proceedings of the AAAI Conference on Artificial Intelligence (AAAI)*, volume 38, pp. 20284–20292, 2024.

Manzil Zaheer, Guru Guruganesh, Kumar Avinava Dubey, Joshua Ainslie, Chris Alberti, Santiago Ontanon, Philip Pham, Anirudh Ravula, Qifan Wang, Li Yang, et al. Big bird: Transformers for longer sequences. *Advances in Neural Information Processing Systems (NeurIPS)*, 33:17283–17297, 2020.

Zhi Zheng, Changliang Zhou, Tong Xialiang, Mingxuan Yuan, and Zhenkun Wang. Udc: A unified neural divide-and-conquer framework for large-scale combinatorial optimization problems. *Advances in Neural Information Processing Systems (NeurIPS)*, 37:6081–6125, 2024.

Jianan Zhou, Yaoxin Wu, Wen Song, Zhiguang Cao, and Jie Zhang. Towards omni-generalizable neural methods for vehicle routing problems. In *International Conference on Machine Learning (ICML)*, pp. 42769–42789. PMLR, 2023.

Zefang Zong, Hansen Wang, Jingwei Wang, Meng Zheng, and Yong Li. Rbg: Hierarchically solving large-scale routing problems in logistic systems via reinforcement learning. In *Proceedings of the 28th ACM Conference on Knowledge Discovery and Data Mining (SIGKDD)*, pp. 4648–4658, 2022.

A PROBLEM FORMULATIONS OF RWVRPS

A.1 VEHICLE ROUTING PROBLEM WITH REPLENISHMENT STOPS (VRP-RS)

The Vehicle Routing Problem with Replenishment Stops (VRP-RS) (Schneider et al., 2015) extends the traditional VRP by incorporating replenishment stops where vehicles can restock goods at intermediate nodes to continue their service. This model accounts for real-world constraints such as maximum driving range limitations due to driver working hours or operational constraints.

Let $\mathcal{V}$ define a set of vehicles, where each vehicle $w \in \mathcal{V}$ has a capacity Q_w. Each customer $n \in \mathcal{N}$ has a demand q_n and $c \in \mathcal{C}$ shows a set of intermediate replenishment stops, which is a subset of $U = \{n_0, n_1, ..., c_1, c_2\}$. The distance between any two nodes i and j, where $i, j \in U$, is shown as d_{ij}. Q defines the maximum vehicle capacity, while the maximum driving range is indicated by R.

Decision variables:

- $x_{ij}^w \in \{0, 1\}$: A binary variable that takes the value 1 if vehicle w travels from node i to node j, and 0 otherwise.
- q_i^w: the load at node i delivered by vehicle w
- r_i^w: the remaining driving range of vehicle w after visiting node i

Problem formulation:

$$\text{Minimize: } \sum_{w \in V} \sum_{i \in U} \sum_{j \in U} d_{ij} x_{ij}^w \tag{11}$$

Where,

All vehicles start and end at the depot:

$$\sum_{j \in U} x_{0j}^w = 1, \quad \sum_{i \in U} x_{i0}^w = 1, \quad \forall w \in \mathcal{V} \tag{12}$$

Every customer must be visited exactly once:

$$\sum_{w \in \mathcal{V}} \sum_{j \in U} x_{ij}^w = 1, \quad \forall i \in \mathcal{N} \tag{13}$$

At each node, the number of incoming and outgoing flows must match:

$$\sum_{i \in U} x_{ij}^w = \sum_{k \in U} x_{jk}^w, \quad \forall j \in U, \forall w \in \mathcal{V} \tag{14}$$

The capacity limit of each vehicle must be satisfied:

$$q_j^w \leq Q, \quad \forall j \in \mathcal{N}, \forall w \in \mathcal{V} \tag{15}$$

A vehicle's remaining capacity decreases after serving a customer:

$$q_j^w = q_i^w - q_j x_{ij}^w, \quad \forall i, j \in \mathcal{N}, \forall w \in \mathcal{V} \tag{16}$$

The total travel time of each vehicle must not exceed its maximum driving range:

$$0 \leq r_i^w \leq R, \quad \forall i \in U, \forall w \in \mathcal{V} \tag{17}$$

The remaining driving range is updated after each traversal:

$$r_j^w = r_i^w - d_{ij} x_{ij}^w, \quad \forall i, j \in U, \forall w \in \mathcal{V} \tag{18}$$

Traveling from the current node to a customer and then to the depot must not exceed the vehicle's driving range:

$$r_i^w \geq d_{ij} + d_{j0}, \quad \forall i, j \in U, \forall w \in \mathcal{V} \tag{19}$$

Visiting a replenishment stop fully restores the vehicle's capacity:

$$q_j^w = Q, \quad \forall j \in C, \forall w \in \mathcal{V} \text{ such that } \sum_{i \in U} x_{ij}^w = 1 \tag{20}$$

A.2 Electric Vehicle Routing Problem with Charging Stations (EVRP-CS)

The Electric Vehicle Routing Problem with Charging Stations (EVRP-CS) (Koç et al., 2019) extends the VRP by adding a fleet of EVs that have limited driving ranges due to battery constraints. There is also set of charging stations along the routes to maintain operational feasibility.

We use the same notation as VRP-RS for problem formulation, with the key difference being that intermediate stops $c \in \mathcal{C}$ now represent charging stations rather than replenishment stops. EVs must visit these charging stations to recharge their batteries and continue their routes.

Decision variables:

- $x_{ij}^w \in \{0, 1\}$: binary variable that equals 1 if vehicle w travels from i to j, and 0 otherwise
- q_i^w: the load at node i for vehicle w
- r_i^w: the remaining battery range of vehicle w at node i

Problem formulation:

$$\text{Minimize: } \sum_{w \in V} \sum_{i \in U} \sum_{j \in U} d_{ij} x_{ij}^w \tag{21}$$

Where,

All vehicles start and end at the depot:

$$\sum_{j \in U} x_{0j}^w = 1, \quad \sum_{i \in U} x_{i0}^w = 1, \quad \forall w \in \mathcal{V} \tag{22}$$

Every customer must be visited exactly once:

$$\sum_{w \in \mathcal{V}} \sum_{j \in U} x_{ij}^w = 1, \quad \forall i \in \mathcal{N} \tag{23}$$

At each node, the number of incoming and outgoing flows must match:

$$\sum_{i \in U} x_{ij}^w = \sum_{k \in U} x_{jk}^w, \quad \forall j \in U, \forall w \in \mathcal{V} \tag{24}$$

The capacity limit of each vehicle must be satisfied:

$$q_j^w \leq Q, \quad \forall j \in \mathcal{N}, \forall w \in \mathcal{V} \tag{25}$$

A vehicle's remaining capacity decreases after serving a customer:

$$q_j^w = q_i^w - q_j x_{ij}^w, \quad \forall i, j \in \mathcal{N}, \forall w \in \mathcal{V} \tag{26}$$

Each vehicle's battery has a minimum and maximum capacity:

$$0 \leq r_i^w \leq R, \quad \forall i \in U, \forall w \in \mathcal{V} \tag{27}$$

The level of remaining battery is updated after traversing:

$$r_j^w = r_i^w - d_{ij} x_{ij}^w, \quad \forall i, j \in U, \forall w \in \mathcal{V} \tag{28}$$

Traveling from the current node to a customer and then to the depot must not deplete the vehicle's battery:

$$r_i^w \geq d_{ij} + d_{jc}, \quad \forall i, j \in U, \forall w \in \mathcal{V}, \forall c \in \mathcal{C} \tag{29}$$

Whenever an EV visits a charging station, its battery is fully recharged:

$$r_j^w = R, \quad \forall j \in C, \forall w \in \mathcal{V} \text{ such that } \sum_{i \in U} x_{ij}^w = 1 \tag{30}$$

A.3 VEHICLE ROUTING PROBLEM WITH TIME WINDOWS (VRPTW)

The Vehicle Routing Problem with Time Windows (VRPTW) (Kallehauge et al., 2005) extends VRP by incorporating time constraints at customer locations. Each customer must be served within a specified time window, making the problem more realistic for applications such as delivery services, waste collection, and appointment scheduling where timing is crucial.

We use the same notation as VRP-RS for problem formulation, with the key difference being that each demand q_i must be served within a time window $[e_i, l_i]$, where e_i is the earliest service time and l_i is the latest service time. The distance between any two nodes i and j is denoted as d_{ij}, with an associated travel time t_{ij}. Each customer i requires a service time s_i.

Decision variables:

- $x_{ij}^w \in \{0, 1\}$: binary variable that equals 1 if vehicle w travels from node i to node j, and 0 otherwise
- T_i^w: arrival time of vehicle w at node i
- q_i^w: cumulative load of vehicle w after serving node i

Problem formulation:

$$\text{Minimize: } \sum_{w \in \mathcal{V}} \sum_{i \in U} \sum_{j \in U} d_{ij} x_{ij}^w \tag{31}$$

Where,

All vehicles start and end at the depot:

$$\sum_{j \in \mathcal{N}} x_{0j}^w = 1, \quad \sum_{i \in \mathcal{N}} x_{i0}^w = 1, \quad \forall w \in \mathcal{V} \tag{32}$$

Every customer must be visited exactly once:

$$\sum_{w \in \mathcal{V}} \sum_{j \in U} x_{ij}^w = 1, \quad \forall i \in \mathcal{N} \tag{33}$$

At each node, the number of incoming and outgoing flows must match:

$$\sum_{i \in U} x_{ij}^w = \sum_{k \in U} x_{jk}^w, \quad \forall j \in \mathcal{N}, \forall w \in \mathcal{V} \tag{34}$$

The capacity limit of each vehicle must be satisfied:

$$q_j^w = q_i^w + q_j x_{ij}^w, \quad \forall i, j \in U, \forall w \in \mathcal{V} \tag{35}$$

$$q_i^w \leq Q, \quad \forall i \in U, \forall w \in \mathcal{V} \tag{36}$$

Time window constraints must be satisfied:

$$e_i \leq T_i^w \leq l_i, \quad \forall i \in U, \forall w \in \mathcal{V} \tag{37}$$

Time consistency constraints must be satisfied:

$$T_j^w \geq T_i^w + s_i + t_{ij} - M(1 - x_{ij}^w), \quad \forall i, j \in U, \forall w \in \mathcal{V} \tag{38}$$

where M is a sufficiently large constant.

Depot time window is between the range:

$$e_0 \leq T_0^w \leq l_0, \quad \forall w \in \mathcal{V} \tag{39}$$

Decision variables must satisfy non-negativity:

$$x_{ij}^w \in \{0, 1\}, \quad T_i^w \geq 0, \quad q_i^w \geq 0 \tag{40}$$

A.4 ASYMMETRIC VEHICLE ROUTING PROBLEM (AVRP)

The Asymmetric Vehicle Routing Problem (AVRP) (Toth & Vigo, 1999) extends the VRP by allowing the travel cost or distance from node i to j to differ from that of traveling from j to i. This asymmetry reflects real-world urban transportation scenarios, where factors such as traffic congestion, one-way streets, and temporarily closed roads can cause travel times between two nodes to vary depending on the direction.

The key distinction of AVRP with other extensions is that the distance matrix is asymmetric: $d_{ij} \neq d_{ji}$ for some pairs (i, j). This creates a directed graph $G = (U, A)$ where A is the set of directed arcs.

Decision variables:

- $x_{ij}^w \in \{0, 1\}$: binary variable that equals 1 if vehicle w traverses arc (i, j)
- q_i^w: load of vehicle w after serving node i

Problem formulation:

$$\text{Minimize: } \sum_{w \in \mathcal{V}} \sum_{(i,j) \in A} d_{ij} x_{ij}^w \tag{41}$$

Where,

All vehicles start and end at the depot:

$$\sum_{j \in \mathcal{N}} x_{0j}^w = 1, \quad \sum_{i \in \mathcal{N}} x_{i0}^w = 1, \quad \forall w \in \mathcal{V} \tag{42}$$

Every customer visited exactly once:

$$\sum_{w \in \mathcal{V}} \sum_{i \in U, i \neq j} x_{ij}^w = 1, \quad \forall j \in \mathcal{N} \tag{43}$$

The capacity limit of each vehicle must be satisfied:

$$q_j^w = q_i^w + q_j x_{ij}^w, \quad \forall i, j \in U, \forall w \in \mathcal{V} \tag{44}$$

$$q_i^w \leq Q, \quad \forall i \in U, \forall w \in \mathcal{V} \tag{45}$$

Vehicle route continuity:

$$\sum_{j \in \mathcal{N}} x_{0j}^w \leq 1, \quad \sum_{i \in \mathcal{N}} x_{i0}^w \leq 1, \quad \forall w \in \mathcal{V} \tag{46}$$

$$\sum_{i \in U, i \neq j} x_{ij}^w = \sum_{k \in U, k \neq j} x_{jk}^w, \quad \forall j \in \mathcal{N}, \forall w \in \mathcal{V} \tag{47}$$

A.4.1 DATASET GENERATION

To generate asymmetric dataset instances, we implement a directional cost perturbation approach. We randomly select β (asymmetry scaling parameter) customers as origin nodes, then independently select β different customers as destination nodes. For each origin-destination pair, we introduce asymmetry by augmenting the forward travel distance by a random factor uniformly sampled from [1, 1+ γ], where γ = 0.2 in our experiments, while keeping the reverse direction unchanged. This creates directional biases that mirror real-world scenarios such as one-way streets, traffic patterns, or elevation changes.

B PROACTIVE MASKING FUNCTION

A masking function is an essential component in approaches for VRP optimization to restrict the search space and prevent model from generating infeasible solutions. The definition of a masking function varies for each specific problem. In the EVRPCS, infeasibility is defined as selecting an already-visited customer, selecting a customer which violate cargo capacity or entails EV to be out of battery before reaching a CS. In the VRPRS, infeasibility occurs when a previously visited customer is visited again, a customer that violate cargo weight is open to select, or decisions that cause the vehicle to exceed its maximum allowable driving range before returning to the depot.

In standard VRP, at each decision step, we evaluate whether any of the remaining customers can be feasibly visited based on the vehicle's current load and remaining capacity. However, VRPRS introduces additional complexity: a vehicle may lack sufficient driving range to reach any subsequent location after completing its current service, rendering the proposed solution infeasible. Similarly, in EVRPCS, the battery constraint adds another layer of feasibility checking beyond simple capacity constraints. Previous approaches, such as those proposed by Wang et al. (2024), have introduced penalty functions to encourage the agent to autonomously explore the feasible domain and learn to generate valid solutions. While this penalty-based approach shows promise, it significantly expands the search space, resulting in longer convergence times during model training. Furthermore, even after complete training, such models may still produce infeasible solutions, compromising their practical reliability.

To address these limitations, we propose a proactive masking function that preemptively eliminates infeasible actions from the decision space. During the decoding step at time t, any customer or intermediate stop is masked if: (i) the customer has already been visited up to time $t-1$, (ii) visiting the customer would cause the vehicle to exceed its capacity limit, or (iii) the vehicle's remaining battery charge (for EVRPCS) or driving range (for VRPRS) is insufficient to reach the selected node and subsequently travel to the nearest charging station, replenishment stop, or depot.

B.1 PROACTIVE MASKING FUNCTION FOR EVRPCS

For the EVRPCS, let $D = \{n_0\} \cup \mathcal{C}$ define the set containing both the depot and all charging stations, where $\mathcal{C}$ represents the set of charging stations. Let $\wedge$ denote the logical AND operator, $\phi \subset \mathcal{N}$ represent the set of visited customers, and $\mathcal{U}_t(j)$ indicate the masking function for visiting node j at time t when vehicle w is currently at node i. The masking function is defined as:

$$\mathcal{U}_t(j) = \begin{cases} \text{False}, & j \notin \phi \wedge q_i^w + q_j \leq Q \wedge r_i^w \geq d_{ij} + \min\limits_{c \in D} d_{jc} \\ \text{True}, & \text{Otherwise} \end{cases} \tag{48}$$

This formulation ensures that a node j is only selectable if: (1) it has not been visited, (2) serving it would not exceed vehicle capacity, and (3) the vehicle has sufficient battery to reach node j and then travel to the nearest charging facility or depot.

B.2 PROACTIVE MASKING FUNCTION FOR VRPRS

For the Vehicle Routing Problem with Replenishment Stops, let $\mathcal{C}$ define the set of intermediate replenishment stops, n_0 denote the depot node, R represent the maximum driving range of the vehicle, and $\phi \subset \mathcal{N}$ show the set of visited customers. Let r_i^w denote the remaining driving range of vehicle w at node i. The lookahead masking function $\mathcal{U}_t(j)$ for VRPRS, which determines the feasibility of visiting node j at time t when vehicle w is at node i, is defined as:

$$\mathcal{U}_t(j) = \begin{cases} \text{False}, & j \notin \phi \wedge q_i^w + q_j \leq Q \wedge r_i^w + d_{ij} + d_{j0} \leq R \\ \text{True}, & \text{Otherwise} \end{cases} \tag{49}$$

This ensures that a customer can only be selected if visiting them and returning to the depot would not violate the driving range constraint.

C EXPERIMENTS ON VERY LARGE VRP PROBLEMS

We evaluated SEAFormer's scalability on the exceptionally large problem instances proposed by Hou et al. (2022), comprising 5,000 and 7,000 nodes in both VRP and RWVRP settings. The results, presented in Table 4, show that SEAFormer consistently outperforms state-of-the-art methods across all RWVRP configurations and scales. The same holds for standard VRP, where SEAFormer surpasses UDC which is the leading divide-and-conquer approach for large-scale VRPs.

Table 4: Experimental results on very large-scale VRP instances. The best overall performance is shown in bold, and the top learning-based method is shaded. We compare the best-performing baselines that run without encountering out-of-memory errors in a reasonable time. Gaps are measured with respect to the best-performing approach.

METHODS	5K CUSTOMERS			7K CUSTOMERS		
	OBJ.	G(%)	T	OBJ.	G(%)	T
LKH	175	26.7	4.3H	245	30.2	14H
TAM-LKH3	144.6	4.7	35M	196.9	4.67	1H
GLOP-LKH3	142.4	3.11	8M	191.2	1.64	10M
LEHD	140.7	1.88	3H	-	-	-
$\text{UDC}_{250}(\alpha = 1)$	139.0	0.65	15M	188.6	0.26	20M
SEAFORMER	**138.1**	**0.00**	22M	**188.1**	**0.00**	34M

Table 5 presents results for very large-scale RWVRPs. SEAFormer demonstrates exceptional scalability on 5,000- and 7,000-customer instances, achieving the best solutions across all four problem variants while existing methods struggle. For VRPTW, it reduces objectives by 94.3% compared to MTPOMO on 5K instances and is the only method effectively solving 7K instances. In EVRPCS, SEAFormer outperforms specialized methods like EVGAT by 45% on 5K instances and maintains this advantage at 7K scale, with similar results for VRPRS. For AVRP, it achieves a 5.57% improvement over the state-of-the-art solver, highlighting SEAFormer's strong generalizability across different problem types and scales.

Table 5: Performance of SEAFormer on a very large scale RWVRP instances. The best results are bolded while the best learning-based method is highlighted. Gaps are measured with respect to the best-performing approach.

RWVRP	METHODS	5K CUSTOMERS			7K CUSTOMERS		
		OBJ.	G(%)	T	OBJ.	G(%)	T
VRPTW	POMO	997	67.2	28M	-	-	-
	MTPOMO	1158	94.3	30M	1656	110	54M
	SEAFORMER	**596**	**0.00**	33M	**786**	**0.00**	65M
EVRPCS	EVRPRL	272.4	90.3	30M	-	-	-
	EVGAT	207.9	45.2	38M	296.8	50.5	75M
	SEAFORMER	**143.1**	**0.00**	32M	**197.1**	**0.00**	65M
VRPRS	EVRPRL	193.2	64.9	30M	-	-	-
	EVGAT	167.3	42.8	38M	230.6	46.8	75M
	SEAFORMER	**117.1**	**0.00**	32M	**157.1**	**0.00**	65M
AVRP	POMO	244	68	17M	-	-	-
	$\text{UDC}_{250}(\alpha = 1)$	154.8	7.05	14M	208.4	5.57	20M
	SEAFORMER	**144.6**	**0.00**	21M	**197.4**	**0.00**	34M

D EXPERIMENTS ON REAL-WORLD CVRPLIB DATASET

On large-scale CVRPLib instances, SEAFormer demonstrates strong performance. Table 6 shows the gap of different methods relative to the best-known solution. When combined with SGBS, it surpasses state-of-the-art solutions; even without SGBS, SEAFormer is only 0.2% less effective on the largest instances, underscoring the robustness of the proposed approach.

Table 6: Gap to Best Known Solution on CVRPLib real-world Benchmark. The best overall performance is highlighted.

Dataset	GLOP-LKH3	LEHD	UDC_{250}	SEAFormer	SEAFormer-SGBS
Set-X(500, 1000)	16.8%	17.4%	7.1%	7.3%	6.8%
Set-XXL(1000, 10000)	19.1%	22.2%	13.2%	13.3%	-

E CROSS-DISTRIBUTION GENERALIZATION

A key requirement for any neural combinatorial optimization (NCO) solver is the ability to generalize beyond the data on which it was trained (Zheng et al., 2024). To evaluate this property, we assessed SEAFormer on two challenging out-of-distribution settings proposed by Zhou et al. (2023): the Rotation and Explosion distributions of the CVRP, each with 500 and 1,000 customers. As reported in Table 7, SEAFormer demonstrates consistent robustness and strong performance even when faced with large-scale instances that exhibit fundamentally different spatial structures.

Table 7: Cross-distribution generalization on 128 instances from the dataset of Zhou et al. (2023). The best overall result is shown in bold, and the top learning-based result is highlighted.

	Rotation			Explosion		
Method	Obj.↓	Gap	Time	Obj.↓	Gap	Time
HGS	**32.97**	0.00%	8h	**32.87**	0.00%	8h
POMO	64.76	96.4%	1m	58.17	76.9%	1m
Omni_VRP	35.9	8.8%	56.8m	35.65	8.45%	56.8m
ELG	37.31	13.16%	16.3m	36.53	8.1%	16.6m
UDC-$x_{250}(\alpha$=1)	35.14	6.58%	3.3m	35.11	6.81%	3.3m
SEAFormer	35.27	6.97%	1m	35.85	9.06%	1m
SEAFOrmer-SGBS	34.51	4.67%	100m	34.84	5.99%	100m

F ADDITIONAL ABLATION STUDY

F.1 ABLATION ON CLUSTER SIZE AND PARTITIONING ROUNDS: IMPACT ON SOLUTION QUALITY AND MEMORY

One of the main contributions of this paper is CPA with its partitioning rounds and smoothing techniques. Figure 4a demonstrates model accuracy under different partitioning and smoothing settings. The SEAFormer's performance improves with increasing partitioning rounds. The accuracy gap between utilizing CPA with 1 partitioning round (PR) with and without smoothing is 0.15% for VRP1000, validating our smoothing approach's effectiveness. Furthermore, the gap reduction from 0.38% to 0.05% demonstrates the power of our deterministic-yet-diverse partitioning strategy. Notably, performance across different partitioning rounds remains relatively consistent, highlighting SEAFormer's architectural strength which achieves high-quality solutions by deterministically attending to small node groups.

Performance gains come at the cost of higher memory usage. Figure 4b illustrates memory consumption during CVRP1k training with batch size 32 and pomo size 100. As anticipated, increasing partitioning rounds and enabling smoothing raise memory requirements, highlighting the trade-off between computational resources and solution quality.

Figure 5 compares CPA attention memory usage with POMO's standard encoder on CVRP1k in logarithmic scale. CPA achieves a 92% reduction with 20 nodes per cluster and 85% with 100 nodes, relative to full-node attention.

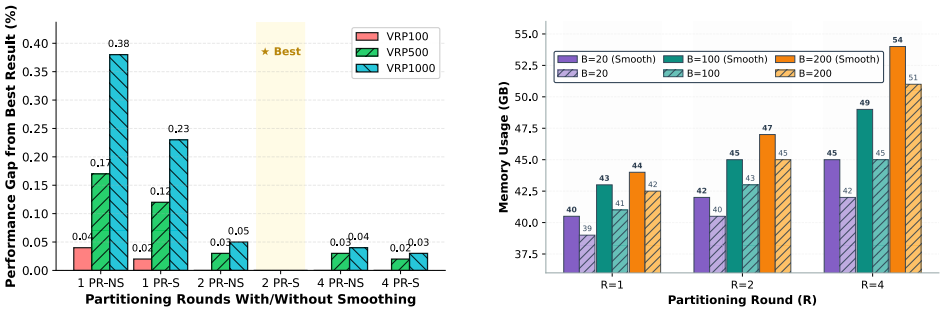

(a) Performance gap for different settings

(b) Training memory consumption

Figure 4: (a) Performance gap of SEAFormer with different CPA configurations. (b) Training memory consumption for a 1,000-node VRP with batch size 32 and pomo size of 100 under different CPA configurations.

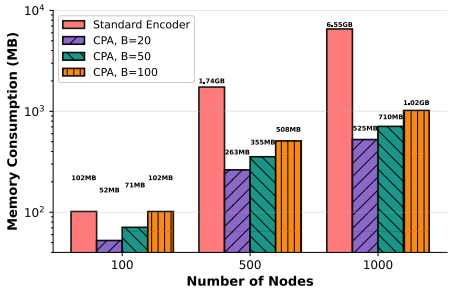

Figure 5: Logarithmic training memory consumption of CPA encoder on a 1,000-node VRP with batch size 32 and pomo size 100 under different configurations.

F.2 Ablation on cluster size and partitioning rounds: impact on convergence

Table 8 examines the convergence behavior of different CPA configurations on VRP100. We report the gap relative to the best objective observed across the entire training process, considering two cluster sizes (20 and 50). In this evaluation, we vary the number of partitioning rounds (PR) and compare settings with smoothing (S) and without smoothing (NS).

The baseline POMO method achieves a 1.19% gap after 1000 epochs. In contrast, our CPA variants consistently deliver stronger performance, with several notable trends. First, the smoothing technique plays a critical role: comparing one partitioning round with and without smoothing reveals gap reductions of 0.51% and 0.45% at epoch 1000 for cluster sizes 20 and 50, respectively. Second, increasing the number of partitioning rounds leads to substantial improvements. For example, moving from one to four rounds with smoothing decreases the final gap from 1.19% to 0.69% for cluster size 20, and from 1.00% to 0.56% for cluster size 50.

We further observe that larger cluster sizes consistently outperform smaller ones across all settings. In particular, cluster size 50 with four partitioning rounds and smoothing achieves the best result, reaching a 0.56% gap. Beyond final performance, CPA also exhibits faster convergence: with four partitioning rounds and cluster size 50, the gap at epoch 100 is already 2.46%, outperforming POMO's performance at epoch 500. This combination of accelerated convergence and superior asymptotic performance highlights the importance of both multiple partitioning rounds and well-chosen cluster sizes within the CPA framework.

Table 8: Performance gap relative to best achieved objective on VRP100 across training epochs with different CPA configurations (PR: Partitioning Rounds, S: Smoothing, NS: No Smoothing)

Method	Cluster size	epoch 100	epoch 500	epoch 1000	Cluster size	epoch 100	epoch 500	epoch 1000
POMO	-	4.16%	1.89%	1.19%	-	-	-	-
1 PR-NS	20	3.97%	2.39%	1.7%	50	3.65%	2.01%	1.45%
1 PR-S	20	3.65%	2.14%	1.19%	50	3.53%	1.57%	1.00%
2 PR-S	20	3.4%	1.51%	0.88%	50	3.15%	1.38%	0.82%
4 PR-S	20	2.58%	1.19%	0.69%	50	2.46%	1.07%	0.56%

F.3 Ablation on edge module effect on AVRP

Table 9 reports the performance gap of SEAFormer without the edge module relative to the full SEAFormer. Across AVRP instances of varying sizes, the gap ranges from 2.4% to 3.4%, highlighting the significant contribution of the edge module to SEAFormer's performance in asymmetric routing settings.

Table 9: Gap between SEAFormer without Edge Embedding (SEAFormer-WOE) and the full SEAFormer on AVRP.

Method	AVRP100	AVRP500	AVRP1000
SEAFormer-WOE	2.4%	2.7%	3.4%

G Optional nodes and their embeddings

SEAFormer treats optional nodes differently from customer nodes for three key reasons. First, the number of optional nodes can change across problem instances, and mixing them with customers could make the customer embeddings unstable. Second, because CPA fixes the number of customers per cluster, adding variable optional nodes would require extra padding, which wastes resources. Third, CPA groups nearby nodes together, so if optional nodes were embedded with customers, some clusters might miss important optional node information, which could hurt solution quality.

For these reasons, we apply self-attention among all optional nodes to capture their inter-relationships. These embeddings are then integrated with customer node representations through a Gumbel-Softmax (Jang et al., 2016) and learnable fusion mechanism. During training, we implement a temperature annealing schedule: τ initializes at 1.0 to encourage exploration and decays by a factor of 0.99 per epoch until reaching 0.2. Through this mechanism, customer embeddings learn to initially explore all optional facilities without bias, then progressively concentrate on the most relevant service nodes as determined by spatial proximity and emerging routing patterns.

H CPA visual example

Figure 6 provides steps of how CPA operates. The input instance (Figure 6a) is first transformed into polar coordinates relative to the depot (Figure 6b). We then compute and normalize the partitioning score from Equation 2 (Figure 6c), sort nodes by that score, and partition them into clusters according to the chosen cluster size (Figure 6d). Finally, Figure 6e compares CPA's attention scores with standard full attention (Figure 6f), highlighting CPA's locality-aware sparsity and its reduced memory footprint.

Figure 7 demonstrates how CPA employs 4 rounds of partitioning with boundary smoothing to generate diverse spatial patterns. This approach preserves the global perspective of problem instances while achieving significant reductions in memory usage and computational cost.

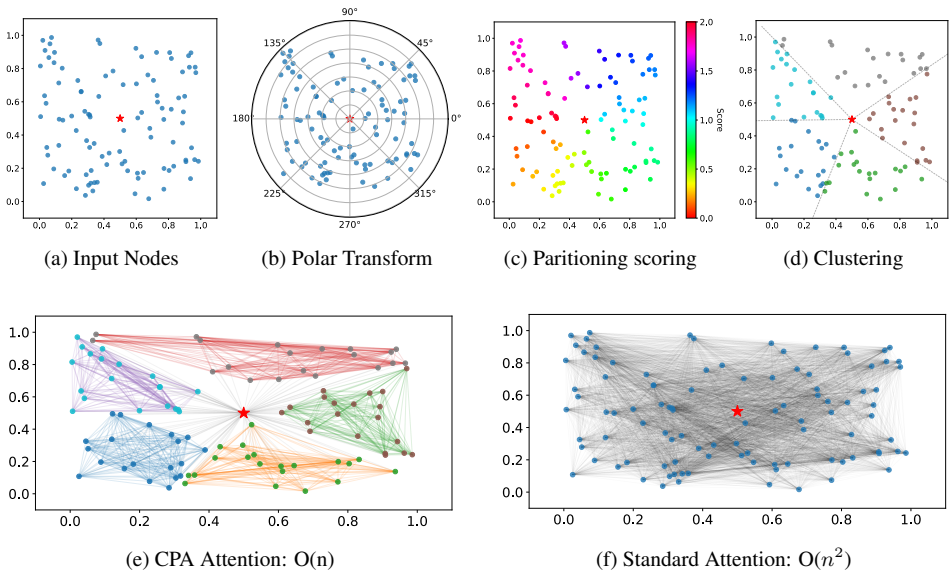

Figure 6: Pipeline of CPA. **Top row**: CPA processing steps - (a) Input nodes in Cartesian space with depot (red star), (b) Polar transformation relative to depot, (c) Angular scoring with $\alpha = 0$ (pure angular), (d) Nodes sorted by angle and partitioned into fixed-size clusters. **Bottom row**: (e) Final CPA attention pattern with O(n) complexity showing attention only within clusters, (f) Standard attention with O(n^2) complexity showing all pairwise connections. CPA reduces number of attention calculation for this example from 10,000 to 2100 (approximately 80% reduction).

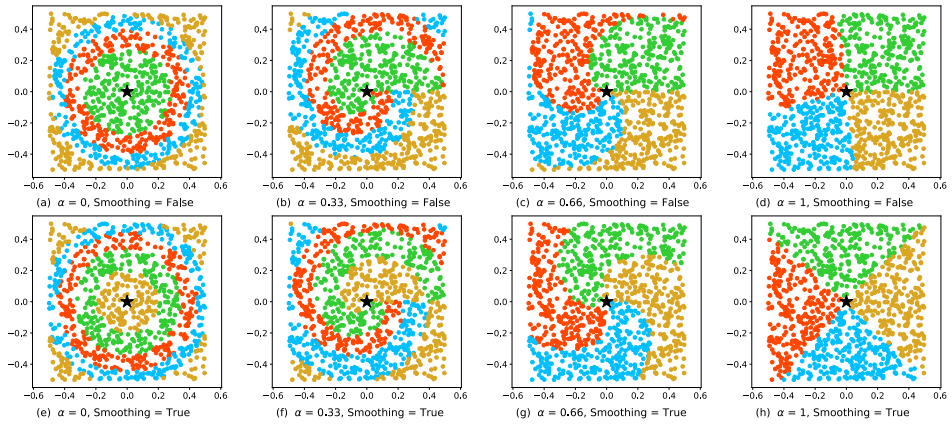

Figure 7: Visualization of Clustered Proximity Attention with $\alpha = [0, 0.33, 0.66, 1]$, where nodes are partitioned into K=4 clusters using polar coordinates centered at the depot (black star). Top row: Without boundary smoothing, hard boundaries can separate nearby nodes. Bottom row: With smoothing, cluster boundaries shift to maintain local neighborhoods. Colors indicate cluster assignment; attention is computed only within same-colored groups plus depot. The mixing parameter α interpolates between radial (α=0) and angular (α=1) clustering, capturing different routing patterns.

I ADDITIONAL RELATED WORK

I.1 CLASSICAL APPROACHES AND THEIR LIMITATIONS

Classical (meta-)heuristic methods for RWVRPs follow a construction-destruction-improvement paradigm. Examples include variable neighborhood search with Tabu search for load-dependent energy consumption (Schneider et al., 2014), ant colony optimization with look-ahead for EVRPCS (Mavrovouniotis et al., 2018), simulated annealing for partial recharging (Felipe et al., 2014), and adaptive large neighborhood search with load-aware power estimation (Kancharla & Ramadurai, 2018). Although these approaches yield high-quality solutions and handle complex constraints, they face two main drawbacks: (i) solution time grows exponentially with problem size (Hou et al., 2022), and (ii) they struggle to generalize, as solutions cannot leverage patterns learned from previous instances. Such limitations make them unsuitable for real-time logistics, where solutions must be produced in seconds rather than hours.

I.2 LEARNING-BASED APPROACHES

The intersection of machine learning and combinatorial optimization has yielded approaches that directly produce high-quality VRP solutions without iterative refinement. These methods fall into two architectural paradigms: (1) Autoregressive models that build solutions sequentially, adding one decision at a time (Khalil et al., 2017; Kool et al., 2018; Kwon et al., 2020; Hou et al., 2022; Luo et al., 2025a; 2023; Zheng et al., 2024; Berto et al., 2025; Nasehi et al., 2025), and (2) Non-autoregressive models that generate complete solutions simultaneously, typically through learned heatmaps (Nowak et al., 2018; Kool et al., 2022; Ye et al., 2024; Xiao et al., 2024). Training paradigms include supervised learning from optimal solutions or reinforcement learning to directly optimize solution quality (Joshi et al., 2019).

Early work by Bello et al. (2016) pioneered learned heuristics using pointer networks trained with actor-critic methods. Nazari et al. (2018) enhanced this framework by incorporating attention mechanisms into the encoder. The field advanced significantly when Kool et al. (2018) applied Transformers to routing problems, demonstrating strong performance across TSP and VRP tasks. Subsequent improvements include POMO (Kwon et al., 2020), which introduced multiple rollouts for better exploration, and multi-decoder architectures (Xin et al., 2021) for enhanced solution refinement. Despite these advances, scaling to large problem instances remains computationally prohibitive.

Divide-and-conquer strategies have emerged as the dominant approach for large-scale instances (Nowak et al., 2018; Li et al., 2021; Zong et al., 2022; Fu et al., 2021; Zheng et al., 2024; Nasehi et al., 2025). TAM (Hou et al., 2022) employs two-stage decomposition followed by LKH3 (Helsgaun, 2017) for sub-problem resolution. GLOP (Ye et al., 2024) integrates global partitioning through non-autoregressive models with local autoregressive construction. UDC (Zheng et al., 2024) addresses sub-optimal partitioning through robust training procedures, combining GNN-based decomposition with specialized sub-problem solvers.

Recently, heavy decoder architectures have emerged as another approach for achieving high-quality results. Luo et al. (2023) proposed shifting computational complexity from the encoder to the decoder, introducing a partial reconstruction approach to enhance model accuracy while maintaining reasonable training times through supervised learning. Luo et al. (2025a) extended this with a boosted heavy decoder variant that restructures attention computation through two intermediate nodes, reducing attention complexity to $O(2n)$. This efficiency gain enables training on significantly larger instances by computing attention from each node to two pivot nodes, then from these pivots to all other nodes, rather than computing full pairwise attention. Huang et al. (2025) provide insights into models with light encoders and identify their weaknesses. They propose RELD, incorporating simple modifications such as adding identity mapping and a feed-forward layer to enhance the decoder's capacity.

J HYPERPARAMETERS

Following previous work (Kwon et al., 2020), we sample depot and customer coordinates uniformly from $[0, 1]^2$ space, with customer demands drawn uniformly from $\{1, ..., 10\}$. Vehicle capacities are

set to 50, 100, and 200 units per Zhou et al. (2023). For each epoch, we generate 10,000 training instances on-the-fly. We train models for 2,000 epochs on 100-customer instances, 200 epochs on 500-customer instances, and 100 epochs on 1,000-customer instances for each problem variant. Training employs batch size 64 with POMO size 100 (Kwon et al., 2020). Our architecture uses a 6-layer encoder with 8 attention heads, embedding dimension 128, and feedforward dimension 512. The learning rate remains fixed at 10^{-4}. We leverage Flash Attention (Dao et al., 2022) in our multi-head attention mechanisms. The edge module uses 32-dimensional embeddings, computing edge representations only between each node and its 50 nearest neighbors as a fixed constraint. All remaining hyperparameters, training algorithms, and loss functions follow POMO (Kwon et al., 2020) specifications.

VRPTW. we follow the time window generation procedure from Liu et al. (2024). Service times and time window lengths are uniformly sampled from [0.15, 0.2], representing normalized time units relative to a planning horizon of T=4.6.

EVRPCS. we randomly select 4 charging stations, and each EV can travel up to 2 units before needing to recharge.

VRPRS. we set 5 replenishment stops, with each vehicle able to travel a maximum of 4 units.

AVRP. the asymmetry scaling parameter β is set to 50, 200, and 400 for 100-, 500-, and 1,000-customer problems, respectively, while the directional bias factor γ is fixed at 0.2 for all instance sizes.

K Baselines, codes and licenses

As noted earlier, many existing methods cannot be directly applied to all RWVRP variants. For EVRPCS, we use two learning-based approaches from the literature, following the implementation details provided in their original papers. To our knowledge, no learning-based solutions exist for VRPRS, so we adapted the EVRPCS methods, given their similarity in implementation and approach, to VRPRS and retrained them. For AVRP, we use baseline methods to generate solutions and then recompute route costs using the asymmetric distance matrix. Reported runtimes reflect only model execution, excluding post-processing or cost recalculation. We keep all hyperparameters at the defaults specified by the original authors. We also include recent concurrent works from arXiv, as well.

OR-Tools. We configure OR-Tools using the PATH_CHEAPEST_ARC strategy to generate initial solutions and apply GUIDED_LOCAL_SEARCH as the local search metaheuristic. The runtime is adapted to problem size, selecting from 30, 180, or 360 seconds per instances. The results reported for OR-Tools are not the optimal, as the process was stopped once the time limit was reached.

HGS. We use the HGS (Helsgaun, 2017) implementation in PyVRP (Wouda et al., 2024) version 0.8.2, setting the neighborhood size to 50, minimum population to 50, and generation size to 100. Runtime is adjusted by problem size, choosing 20, 120, or 240 seconds per instance. All other parameters remain at default. The results reported for HGS are not the optimal, as the process was stopped once the time limit was reached.

The available codes and their licenses for used in this work are listed in Table 10.

L Use of Large Language Models

We use LLM assistance for grammar and presentation improvements. The original text and ideas remain the authors' work, and they take full responsibility for the content.

Table 10: Resources for TSP and Optimization Problems

Resource	Link	License
LKH3 (Helsgaun, 2017)	http://webhotel4.ruc.dk/keld/research/LKH-3/	Academic research use
HGS (Vidal, 2022)	https://github.com/chkwon/PyHygese	MIT License
PyVRP (Wouda et al., 2024)	https://github.com/PyVRP/PyVRP	MIT License
POMO (Kwon et al., 2020)	https://github.com/yd-kwon/POMO	MIT License
LEHD (Luo et al., 2023)	https://github.com/CIAM-Group/NCO_code/tree/main/single_objective/LEHD	MIT License
BLEHD (Luo et al., 2025a)	https://github.com/CIAM-Group/SIL	MIT License
ELG (Gao et al., 2024)	https://github.com/lamda-bbo/ELG	MIT License
GLOP (Ye et al., 2024)	https://github.com/henry-yeh/GLOP	MIT License
DeepMDV (Nasehi et al., 2025)	https://github.com/SaeedNB/DeepMDV	MIT License
RELD (Huang et al., 2025)	https://github.com/ziweileonhuang/reld-nco	-
UDC (Zheng et al., 2024)	https://github.com/CIAM-Group/NCO_code/tree/main/single_objective/UDC-Large-scale-CO-master	MIT License